Chinese Chemical Letters 37 (2026) 111836

Contents lists available at ScienceDirect

Chinese Chemical Letters

journal homepage: www.elsevier.com/locate/cclet

A heterogeneity-modulated hydrogel for acute and chronic colitis therapy

Yu-Yang Bi[a,b,1], Ling-Feng Zhang[b,1], Qiu Chen[b], Ming-Yuan Yang[b], Lei Xing[b], Hu-Lin Jiang[a,b,c,d,*], Xian-Wu Cheng[a,*]

[a] Provincial Key Laboratory of Stress and Cardiovascular Disease, Department of Cardiology and Hypertension, Yanbian University Hospital, Yanji 133000, China
[b] State Key Laboratory of Natural Medicines, Department of Pharmaceutics, China Pharmaceutical University, Nanjing 210009, China
[c] Joint International Research Laboratory of Target Discovery and New Drug Innovation, MOE, Nanjing 210009, China
[d] Department of Precision Medicine, School of Medicine, Sungkyunkwan University, Suwon 16419, South Korea

ARTICLE INFO

Article history:
Received 2 July 2025
Revised 11 September 2025
Accepted 12 September 2025
Available online 13 September 2025

Keywords:
Inflammatory bowel disease
Oral drug delivery
Hydrogel
Neutrophils
Macrophages
Reactive oxygen species

ABSTRACT

Inflammatory bowel disease (IBD) exhibits pathological heterogeneity driven by multifactorial origins and patient variability, posing therapeutic challenges due to divergent immune microenvironment dynamics. Notably, neutrophils and macrophages showed prominent heterogeneity in IBD patients and underwent different reprogramming during the acute and chronic inflammatory phases. To address this pathological complexity, an orally administered TH@PVP-gel system integrating tanshinone IIA (Tan) and hemin (Hem) was engineered to address the heterogeneity of IBD pathology with the aim of achieving multi-targeted modulation of IBD. TH@PVP-gel specifically promoted neutrophil apoptosis and facilitated macrophage M2 polarization in the inflamed environment of the colon, targeting inflammatory heterogeneity and remodeling the inflammatory environment. In addition, the TH@PVP-gel efficiently scavenged reactive oxygen species (ROS), inhibited the death of colonic epithelial cells, and restored the intestinal barrier. Ultimately, the TH@PVP-gel demonstrated excellent therapeutic efficacy in both acute and chronic colitis, providing a potential strategy for the broad-spectrum treatment of IBD.

© 2026 Published by Elsevier B.V. on behalf of Chinese Chemical Society and Institute of Materia Medica, Chinese Academy of Medical Sciences.

Inflammatory bowel disease (IBD) is a chronic, nonspecific inflammatory disease of the intestines that mainly includes two types: ulcerative colitis (UC) and Crohn's disease (CD) [1]. In recent years, with improvement in living standards and changes in dietary habits, an increasing number of patients have been diagnosed with IBD, and its incidence is increasing globally, with the current prevalence of IBD as high as 0.5% in Western countries [2,3]. The treatment of IBD is mainly at achieving remission and maintenance therapy and requires long-term medication. Traditional therapeutic agents include 5-aminosalicylic acid (5-ASA), glucocorticoids, and immunosuppressive agents [4]. However, these drugs are limited by side effects, drug resistance and poor adaptation to disease heterogeneity [5,6]. In addition, IBD pathogenesis exhibits significant interpatient and intrapatient variability across disease stages, and multiple pathologic factors and heterogeneity among patients make the treatment of IBD extremely difficult. Conventional monotherapeutic approaches targeting isolated pathways frequently fail to address the spectrum of molecular mechanisms driving diverse treatment responses, ultimately limiting their broad-spectrum efficacy in heterogeneous IBD populations [7].

IBD is characterized by a complex pathology in which neutrophil-macrophage-reactive oxygen species (ROS) interact to drive a self-perpetuating inflammatory cycle with temporal and spatial variations [8,9]. Sustained activation and over-recruitment of neutrophils are characteristic symptoms of IBD [10], and these activated neutrophils release proteolytic hydrolases and produce excessive ROS, which not only directly damage the intestinal epithelium but also contribute to the polarization of macrophages toward the pro-inflammatory M1 phenotype [11,12]. In turn, M1-type macrophages recruit more neutrophils by secreting chemokines and producing ROS *via* nicotinamide adenine dinucleotide phosphate (NADPH) oxidase activity, thereby further amplifying inflammation and creating a self-reinforcing cycle of inflammation and oxidative stress [13–15]. Under physiological conditions, apoptotic neutrophils are cleared by macrophages *via* phagocytosis, a process that promotes macrophage reprogram-

* Corresponding authors.
E-mail addresses: jianghulin3@cpu.edu.cn (H.-L. Jiang), chengxw@ybu.edu.cn (X.-W. Cheng).
[1] These authors contributed equally to this work.

https://doi.org/10.1016/j.cclet.2025.111836
1001-8417/© 2026 Published by Elsevier B.V. on behalf of Chinese Chemical Society and Institute of Materia Medica, Chinese Academy of Medical Sciences.

ming toward the M2 phenotype to alleviate inflammation [16–23]. Conversely, impaired neutrophil apoptosis impacts this process, preventing the transition to M2 macrophages and trapping macrophages in a pro-inflammatory state that sustains ROS production and neutrophil recruitment [24–27]. Notably, the myeloid compartment, including neutrophils and macrophages, shows the greatest compositional diversity in the patient population, suggesting that these cell types contribute to differences in disease phenotype and progression over time between patients. On the basis of the heterogeneity of neutrophils and macrophages in the patient population, neutrophil-macrophage-ROS interactions in the progression of inflammation are therefore differentiated.

Based on these studies, the heterogeneity of acute and chronic colitis was examined in our work. The experimental results demonstrating the imbalance that arises in the different processes of IBD-the heterogeneity of neutrophils *versus* macrophages in acute and chronic colitis, highlights the need for adaptive therapeutic strategies. In existing therapeutic studies of IBD, neutrophils or macrophages are usually regulated individually to alleviate inflammation, but precisely regulating the function of both cell types simultaneously remains a major challenge. The use of antioxidants to scavenge ROS in the gut is one of the key therapeutic approaches for the treatment of IBD; however, antioxidant monotherapy alone is insufficient, as it addresses only the downstream oxidative consequences but not the cellular source of ROS production, the dysregulated interactions between neutrophils and macrophages. While recent studies have explored strategies such as drug co-delivery nanoparticles [28], ROS-scavenging materials [29], or colon-targeted hydrogels [30] for IBD therapy, these approaches often modulate one or two pathological facets or lack a mechanism designed to dynamically adapt to the evolving neutrophil-macrophage-ROS axis across acute and chronic disease stages. The natural compounds tanshinone IIA (Tan) and hemin (Hem) target all three axes of pathology simultaneously, providing a potential solution. Tan specifically induces neutrophil apoptosis, thereby reducing ROS production by neutrophils and forming apoptotic bodies that contribute to macrophage polarization toward the M2 phenotype [31–33]. Hem complements this effect by directly scavenging ROS through its iron porphyrin structure while inhibiting the activation of M1-type macrophages [34,35]. This specific dual-compound synergy targeting neutrophil apoptosis induction, M1 macrophage inhibition, and ROS scavenging represents a distinct multi-axial strategy. However, the therapeutic potential of this combination is diminished by its poor solubility and inability to be delivered in a targeted manner to inflamed intestinal regions [36–40]. Effective therapy must simultaneously modulate neutrophil apoptosis, macrophage plasticity and ROS dynamics and adapt to disease progression.

In this study, the heterogeneity of IBD was addressed by a multi-targeted remodeling of the inflammatory environment to achieve a stronger broad-spectrum IBD therapy. To ameliorate the problems associated with the use of Tan and Hem in the oral treatment of IBD [41–43], PVP-coated TH@PVP NPs self-assembled from Tan and Hem were constructed to increase the stability of the nanoparticles under acidic and basic conditions [44]. To further enhance the oral delivery efficiency of TH@PVP NPs and drug enrichment in the colon, TH@PVP NPs were further loaded into a sodium alginate hydrogel to obtain TH@PVP-gel, which could effectively target the release of nanoparticles at the colon site (Fig. 1) [45,46]. This design integrates nanoparticle stabilization within a colon-targeting hydrogel, creating a composite system specifically enabling the oral delivery and targeted release of the synergistic combination. The dual-phase action of the TH@PVP-gel adapts to disease progression: in acute inflammation, targeting overactive neutrophils reduces ROS bursts and neutralizes residual ROS, breaking the neutrophil-M1 macrophage amplification cycle and

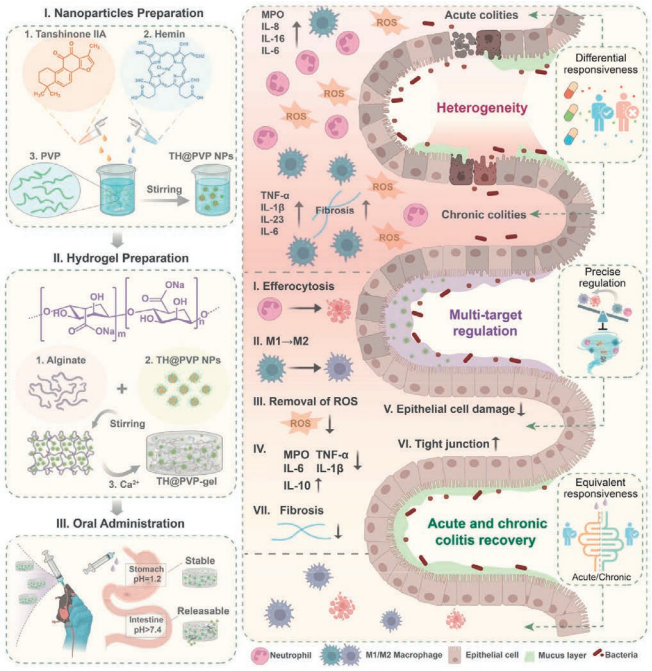


Fig. 1. Schematic illustration of the construction of a hydrogel oral delivery system for the colon-responsive release process and treatment of IBD.

attenuating epithelial damage; in chronic inflammation, it continuously promotes neutrophil clearance, restores macrophage M2 polarization, and inhibits M1 activity to reduce fibrosis. This adaptive therapeutic logic, leveraging coordinated action on neutrophils, macrophages, and ROS to achieve stage-specific effects. Owing to its multi-targeting mechanism, TH@PVP-gel could ultimately effectively inhibit the inflammatory response and promote the repair of damaged tissues in acute and chronic IBD models, which has clinical therapeutic potential for the broad-spectrum treatment of IBD, which has complex pathological features and large individual differences in patients.

IBD makes the treatment of the disease difficult because of its complex pathological features, and commonly used clinical therapeutic agents are often unresponsive in the treatment of many patients. Currently, some studies have been conducted to further understand the complex pathological features of IBD patients by examining the heterogeneity of immune cells in the inflammatory milieu in some samples from healthy individuals or IBD patients. Colonic biopsies from healthy people, UC patients, and CD patients revealed that neutrophils and macrophages presented the most obvious heterogeneity, which may be significantly associated with differences between different stages of the disease or between different individuals. On the basis of these basic studies, we examined several pathological features as well as the number of neutrophils and macrophages in an acute/chronic colitis mouse model of with the application of dextran sulfate sodium (DSS). First, hematoxylin and eosin (H&E), Masson, and terminal-deoxynucleotidyl transferase mediated nick end labeling (TUNEL) staining were performed on healthy samples and samples from different stages of inflammation (Fig. 2A). Compared with those in healthy mice, many inflammatory cells were observed in the mucosal layer and submucosal layer in acute colitis, and the crypts were deformed and destroyed; epithelial hyperplasia, granulation tissue hyperplasia, and colonic mucosal erosion were observed in chronic colitis. Intestinal fibrosis is usually the result of chronic inflammation, a common complication of IBD, as shown in Fig. 2A, and the degree of fibrosis differs between acute and chronic in-

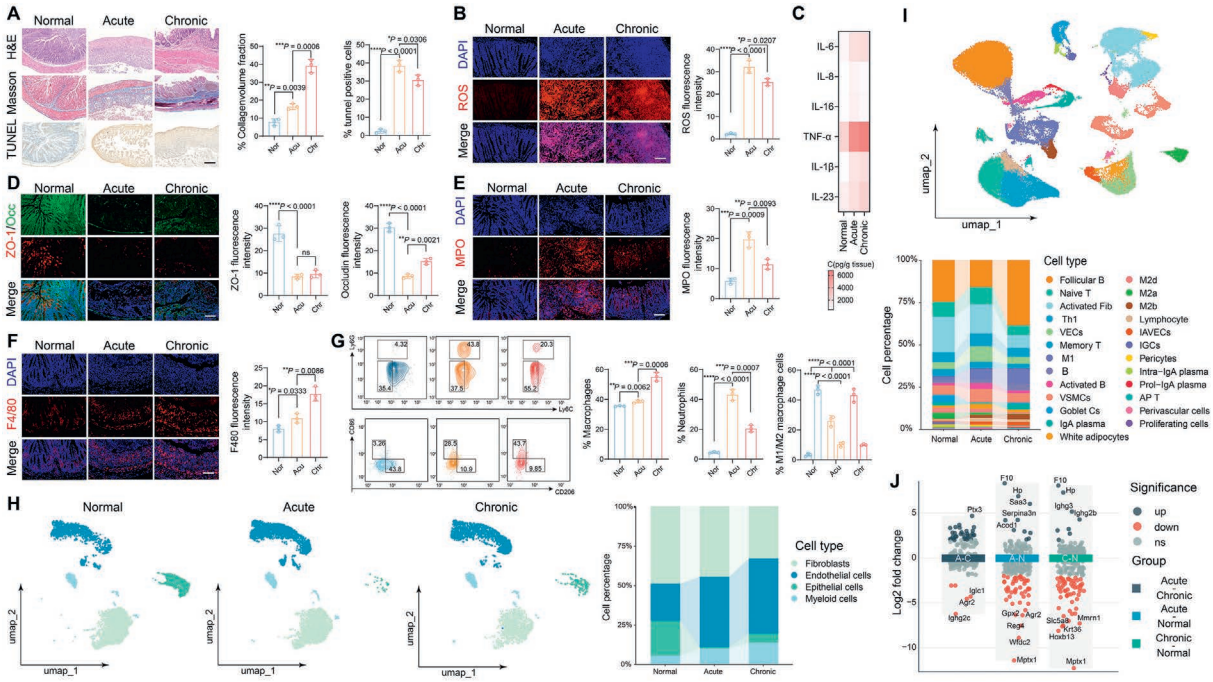


Fig. 2. Heterogeneity of acute and chronic inflammatory environments in the colon. H&E, Masson, and TUNEL staining (A) and confocal images of ROS in the colon tissues of each group. (B) Confocal images of ROS in the colon tissues of mice in each group after treatment. (C) Heatmap of the IL-6, IL-8, IL-16, TNF-α, IL-1β and IL-23 expression profiles in serum ($n = 3$ mice per group). (D) Confocal images of ZO-1 and occludin in the colon tissues of mice in each group after treatment. Confocal images of myeloperoxidase (MPO) (E) and F4/80 (F) expression in the colon tissues of mice after treatment in each group. (G) The number of neutrophils/macrophages in the colon and the proportion of M2 macrophages in the colon were analyzed *via* FACS. Scale bar: 100 μm. Data are shown as the mean ± SD ($n = 3$ independent samples; one-way ANOVA followed by Tukey's HSD *post hoc* test). n.s., no significance. (H, I) Uniform Manifold Approximation and Projection (UMAP) plots showing all mouse cell populations by major cell type and condition; bar plot showing the results of the cell type enrichment analysis. (J) Volcano plot of differentially expressed genes (DEGs) comparing in each group.

flammation, with chronic colitis resulting in increased collagen deposition. In addition, various patterns of programmed cell death are elevated during active intestinal episodes in patients with IBD, and TUNEL staining revealed a greater degree of apoptosis in the intestinal epithelium during acute inflammation. While ROS were also examined as one of the factors contributing to the damage caused to epithelial cells in the inflammatory milieu, ROS levels were slightly higher in acute inflammatory colon tissues than in chronic inflammatory colon tissues (Fig. 2B). The expression of inflammatory factors also differed between acute and chronic colitis tissues (Fig. 2C), suggesting that the responsiveness of single-target-based targeted modulation can vary from patient to patient. Next, the expression of the tight junction proteins occludin and zonula occludens-1 (ZO-1), which are regulators of epithelial proliferation and survival, was examined. As shown in Fig. 2D, the intestinal barrier was damaged to varying degrees in both acute and chronic colitis tissues. On the basis of the heterogeneity of neutrophils and macrophages reported in previous studies, the ratio of neutrophils to macrophages in the colonic tissues of acute and chronic colitis tissues mice was examined *via* immunofluorescence (IF) and fluorescence-activated cell sorting (FACS), respectively. The results of IF staining for markers of neutrophils and macrophages revealed greater infiltration of neutrophils in acute colitis and of macrophages in chronic colitis (Figs. 2E and F). Next, both the number of both types of cells and the number of M1/M2 macrophages were examined *via* FACS (Fig. 2G and Fig. S1 in Supporting information), further confirming the heterogeneity of acute and chronic colitis.

Next, to further analyze the heterogeneity of acute and chronic colitis, we analyzed the raw data from the Gene Expression Omnibus (GEO) database (GSE264408). To characterize the changes in the cellular composition during inflammation visually, we quantified the proportions of the major cell types involved in acute and chronic colitis (Fig. 2H). Consistent with the results of the previous experiments, a dramatic reduction in the epithelial cell population in acute colitis reflected tissue damage, and a partial reversal of epithelial barrier disruption as well as an increase in the degree of fibrosis was observed in chronic colitis compared with acute colitis. In addition, the number of myeloid cells containing neutrophils and macrophages differed between acute and chronic colitis. Next, the major cell types involved in acute and chronic colitis were further subdivided (Fig. 2I), and the results were consistent with the results of FACS, which revealed more macrophages, especially M1-type macrophages, in chronic colitis. In addition, macrophages in different groups were also analyzed for differential gene expression, as shown in Fig. 1J, further demonstrating the complexity of inflammation-targeted therapies cause by heterogeneity. Preliminary examination of the pathological features of the different processes of inflammation and the immune environment revealed some of the same and different characteristics of acute and chronic colitis. Multi-target remodeling of the inflammatory milieu by addressing these characteristics may serve as a novel therapeutic option to improve the lack of responsiveness of single targets in the clinical management of IBD patients.

Tan and Hem can synergistically remodel the IBD immune microenvironment and both act as antioxidants to scavenge ROS in the gut; however, the extremely low water solubility and bioavailability of Tan and Hem lead to poor catalytic activity. To address this problem, PVP-encapsulated dual-drug self-assembled nanoparticles (TH@PVP NPs) of Hem and Tan were prepared *via* the reverse solvent method (Figs. 3A and B), and the optimal ratio of Hem to Tan was determined by the encapsulation rate, particle size, and polymer dispersity index (PDI). The experimental results are shown in Fig. 3C. When the mass ratio of Hem to Tan was 2:1, various metrics, such as the encapsulation rate, reached their optimum values. This ratio was chosen as the final ratio, and the encapsulation

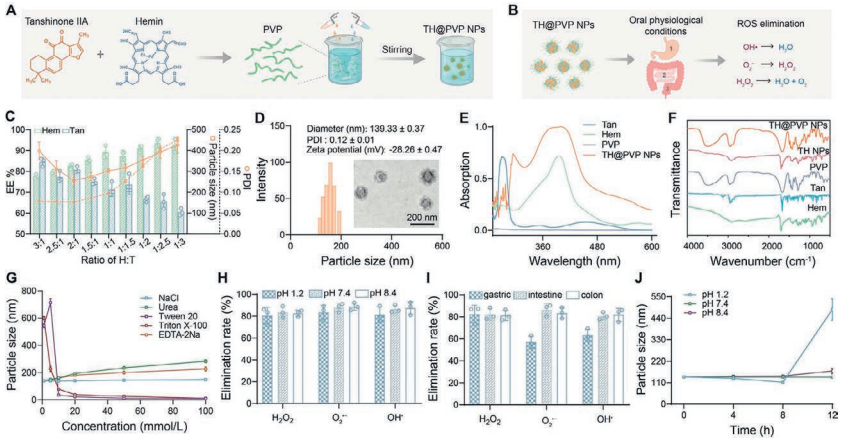


Fig. 3. Preparation of TH@PVP NPs and characterization of their *in vitro* ROS scavenging activity. (A) Preparation process and (B) ROS scavenging ability of TH@PVP NPs. (C) Encapsulation efficiency, particle size, and PDI of nanoparticles formed with different proportions of Hem and Tan. (D) Particle size, PDI, zeta potential, and transmission electron microscope (TEM) image of the TH@PVP NPs. Scale bar: 200 nm. (E) UV–vis spectra of Tan, Hem, PVP, and TH@PVP NPs. (F) Fourier transform infrared absorption spectra of TH@PVP NPs, TH NPs, PVP, Tan, and Hem. (G) Self-assembly mechanism of TH@PVP NPs. Efficiency of ROS scavenging by TH@PVP NPs at different pH values (H) or in different digestion solutions (I). (J) Changes in the particle size of TH NPs under different pH conditions. Data are shown as the mean ± SD ($n = 3$ independent samples).

rates of Hem and Tan were 82.51 % ± 1.04 % and 80.73 % ± 1.18 %, respectively. The DLS results reveal that the average particle size of the TH@PVP NPs was 139.33 ± 0.37 nm, with a zeta potential of −28.26 ± 0.47 mV. The average particle size of the TH NPs with unencapsulated PVP was 113.65 ± 0.29 nm, and the zeta potential was −15.83 ± 0.67 mV, demonstrating the successful encapsulation of PVP (Fig. 3D and Fig. S2 in Supporting information). To further demonstrate the successful preparation of TH@PVP NPs, TH@PVP NPs were characterized *via* UV–vis spectroscopy and Fourier transform infrared (FTIR) spectroscopy. The UV–vis results revealed that TH@PVP NPs had characteristic absorption peaks for both Hem and Tan (Fig. 3E). The FTIR results, as shown in Fig. 3F, revealed that the characteristic absorption peaks of the TH@PVP NPs were different from those of the TH NPs, which were masked by the characteristic absorption peaks of PVP, further confirming the successful wrapping of PVP. In addition, the mechanism of the self-assembly of TH@PVP NPs and TH NPs was examined, and hydrophobic forces were the main force for the formation of TH@PVP NPs, whereas ligand bonding and hydrogen bonding forces had a greater influence on TH NPs (Fig. 3G and Fig. S3 in Supporting information).

Moreover, the ROS scavenging ability of the TH@PVP NPs and TH NPs was also examined *in vitro*, and the experimental results revealed that the TH@PVP NPs were more efficient than the TH NPs at scavenging hydrogen peroxide (H_2O_2), superoxide anions ($O_2^{\bullet -}$) and hydroxyl radicals ($OH^{\bullet}$) at pH values of 1.2 and 8.4 and in different digestive fluids, which confirmed that the TH@PVP NPs had a greater ROS scavenging capacity due to their stability in the GI tract (Figs. 3H and I, Fig. S4 in Supporting information). Finally, the stabilities of the TH@PVP NPs and TH NPs at different pH values were also examined separately, and the TH NPs were found to be unstable at both pH 1.2 and 8.4, whereas the encapsulation of PVP significantly improved the stability of the nanoparticles during the oral digestion (Fig. 3J and Fig. S5 in Supporting information).

To further enhance the potential of TH@PVP NPs for oral application, TH@PVP NPs were loaded into hydrogels of sodium alginate to protect TH@PVP NPs from harsh gastric conditions and achieve pH-responsive drug release in the intestine. The TH@PVP-gel was prepared *via* the method shown in Fig. 4A, and the hydrogel loaded with TH@PVP NPs was successfully prepared after the addition of Ca^{2+} for cross-linking. Next, the elemental distribution and morphology of the TH@PVP-gel were further investigated by scanning electron microscopy (SEM). The results revealed that the elements C, H, O, Na, Fe, Ca, and N were uniformly distributed

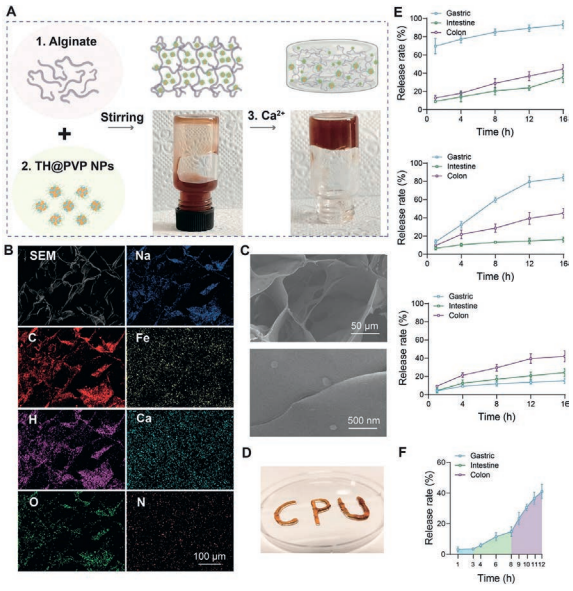


Fig. 4. Preparation of the TH@PVP-gel and examination of its *in vitro* release behavior. (A) Preparation process and photographs of the TH@PVP-gel. (B) EDS element mapping of the TH@PVP-gel. Scale bar: 100 μm. (C) SEM image of the TH@PVP-gel. Scale bar: 50 μm and 500 nm. (D) Validation of the injectability of the TH@PVP-gel. (E) Release profiles of the TH NPs (i), TH@PVP NPs (ii), and TH@PVP-gel (iii) in different digestion solutions. (F) Model of the release profile of the TH@PVP-gel during oral administration. Data are shown as the mean ± SD ($n = 3$ independent samples).

in the TH@PVP-gel, which resulted in a three-dimensional mesh structure in which nanoparticles were loaded (Figs. 4B–D). In the next step, the release of TH NPs, TH@PVP NPs, and TH@PVP-gel on Hem in different digestion solutions was examined. The results, as shown in Fig. 4E, revealed that TH NPs were rapidly released into the gastric fluid, that TH@PVP NPs were released into the gastric fluid at a slower rate than were TH NPs, and that TH@PVP-gel maximally slowed the release of the drug in the gastric fluid. Furthermore, TH@PVP-gel was released fastest in the colon. These results further suggest that the encapsulation of PVP enhances the stability of the nanoparticles in the gastric fluid environment, whereas sodium alginate hydrogel further enhances the stability in the gastric fluid environment and can be released faster in the colon due

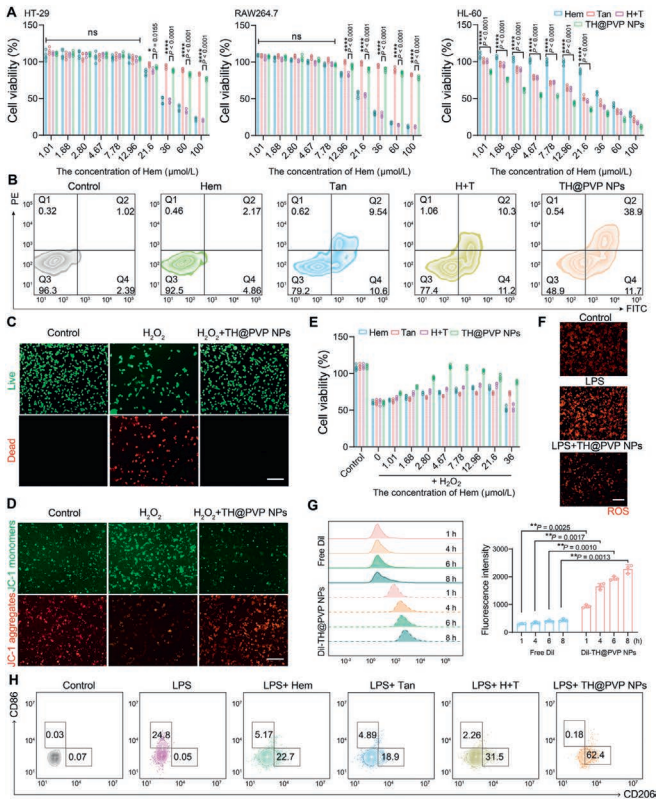


Fig. 5. Anti-inflammatory mechanisms of TH@PVP NPs *in vitro*. (A) Cytotoxicity of various formulations in cells after 24 h of incubation ($n = 5$ independent samples). (B) Inverted microscopy images of HT-29 cells subjected to calcein AM/PI double staining after 6 h of treatment with 4 μmol/L different formulations and (C) inverted microscopy images of JC-1 in HT-29 cells treated with 4 μmol/L different formulations for 6 h (dose based on Tan; $n = 3$ independent samples). (D) Cytotoxicity of various formulations in HT-29 cells after 24 h of incubation (dose based on Tan; $n = 5$ independent samples). (E) Inverted microscopy images of ROS in HT-29 cells treated with 4 μmol/L different formulations for 6 h (dose based on Tan; $n = 3$ independent samples). (F) FACS quantification of the uptake of DiI-TH@PVP NPs for different durations in HT-29 cells. (G) The apoptosis rate of HL-60 cells after incubation with 4 μmol/L different formulations (dosage based on Tan) for 6 h was determined by FACS analysis, and (H) detection of M1/M2 macrophages *via* FACS ($n = 3$ independent samples). Scale bar: 100 μm. Data are shown as the mean ± SD (one-way ANOVA followed by Tukey's HSD *post hoc* test).

to pH changes [47]. Finally, release during digestion was simulated *in vitro*, as shown in Fig. 4F. TH@PVP-gel was released slowly in the gastric and small intestinal fluids during the first 8 h, while the release was accelerated in the colonic fluids after 8 h, which could effectively achieve on-demand release of the drug.

First, cytotoxicity experiments were performed using HT-29 cells, RAW264.7 cells, and HL-60 cells, which are the three commonly used cell lines to study colonic tissue epithelial cells, macrophages, and neutrophils, respectively, to assess the biocompatibility and cellular-level anti-inflammatory mechanism of the TH@PVP NPs. As shown in Fig. 5A, for HT-29 cells and RAW264.7 cells, the formation of Hem dimers was prevented by the self-assembly of TH@PVP NPs, thereby alleviating the safety concerns associated with the potential toxicity of high doses of Hem [48]; for HL-60 cells, Tan specifically induced apoptosis, whereas TH@PVP NPs induced HL-60 to a greater extent of apoptosis. Next, the ability of TH@PVP NPs to induce apoptosis in HL-60 cells was further examined *via* an apoptosis assay, and the results were consistent with the cytotoxicity assay, which revealed that TH@PVP NPs effectively induced apoptosis in HL-60 cells (Fig. 5B and Fig. S6 in Supporting information).

Previous studies have shown that Hem can effectively scavenge ROS based on its porphyrin structure, whereas Tan can inhibit ROS production and increase superoxide dismutase (SOD) activity to scavenge ROS through a reverse electron transfer mechanism. Therefore, the ability of TH@PVP NPs to protect against ROS-induced injury in epithelial cells and the ability to scavenge ROS were further investigated. First, HT-29 cells induced with H_2O_2 and treated with TH@PVP NPs were double-stained with calcein acetoxymethyl ester (calcein AM)/propidium iodide (PI). The results showed that TH@PVP NPs treatment significantly alleviated the death of epithelial cells caused by H_2O_2 treatment (Fig. 5C). To further verify these results, HT-29 cells induced with H_2O_2 and treated with TH@PVP NPs were stained with JC-1 (mitochondrial membrane-potential dye). H_2O_2 treatment led to mitochondrial depolarization in epithelial cells and thus early apoptosis, which was significantly alleviated by TH@PVP NPs treatment (Fig. 5D and Fig. S7 in Supporting information). In addition, the results were further validated *via* a cytotoxicity assay in HT-29 cells, and the results were consistent with previous results showing that TH@PVP NPs could protect intestinal epithelial cells from damage in the inflammatory environment (Fig. 5E). ROS staining was performed on HT-29 cells after lipopolysaccharide (LPS) treatment and TH@PVP NPs treatment (Fig. 5F and Fig. S8 in Supporting information), and the results revealed that the intracellular ROS content in epithelial cells was elevated in the inflammatory environment and that the TH@PVP NPs effectively scavenged excessive intracellular ROS.

Next, the uptake of TH@PVP NPs was examined in each of the three cell types. Compared with that of free DiI (1,1′-dioctadecyl-3,3,3′,3′-tetramethylindocarbocyanine perchlorate), the uptake of TH@PVP NPs by the three cell lines was significantly greater, and the uptake increased continuously with time (Fig. 5G and Fig. S9 in Supporting information). Finally, the therapeutic effects of TH@PVP NPs and other control treatments on LPS-induced M1 polarization of macrophages were also examined. As shown in Fig. 5H and Fig. S10 (Supporting information), both Hem and Tan promoted macrophage M2 polarization, while the TH@PVP NPs had the most significant therapeutic effect. On the basis of the mechanism of the anti-inflammatory effects of TH@PVP NPs *in vitro*, it can be concluded that TH@PVP NPs can promote neutrophil-specific apoptosis, clear ROS, protect intestinal epithelial cells, and promote M2 macrophage polarization more effectively than Tan. These results suggest that TH@PVP NPs can be used as a multi-targeted therapy for IBD, providing an integrated treatment for complex pathological features.

The use of drinking water containing DSS is a method for constructing mouse models mimicking human IBD, where the *in vivo* distribution of orally administered TH@PVP-gel was investigated by constructing DSS-induced acute colitis model mice (all animal experiments were approved by the Regional Ethics Committee of China Pharmaceutical University with the number of 2024–10–085). Next, the biodistribution of the TH@PVP-gel was further examined *in vivo* on the basis of its good performance for oral application in an *in vitro* simulated release assay. First, nanoparticles encapsulating DiR (1,1′-dioctadecyl-3,3,3,3′-tetramethylindotricarbocyanine iodide) or DiI were prepared and further loaded into the hydrogels, and the animals were modeled and treated according to the experimental protocol, as shown in Fig. 6A. Imaging analyses were carried out *in vivo* and *ex vivo* at 2, 6, 10, and 24 h after the administration of the TH@PVP-gel. As shown in Figs. 6B and E, free DiR gradually reached the colon from the stomach at 2–6 h after oral administration, and reached the highest value at ~10 h. In addition, the fluorescence intensity observed in the colon decreased, whereas the fluorescence intensity of TH@PVP-gel loaded with DiR in the GI tract changed similarly to that of free DiR during the first 6 h. The fluorescence intensity detected in the colon was higher at the 10th h than that of free DiR, and the fluorescence intensity did not decrease significantly at 10–24 h. This result indicated that the drug accumulation at the

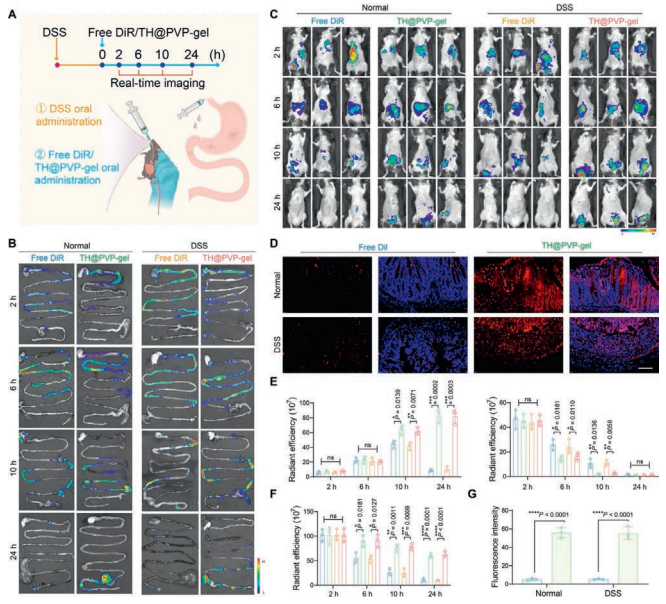


Fig. 6. Biodistribution of the TH@PVP-gel. (A) Schematic diagram of the biodistribution examination. (B) Representative *ex vivo* biodistribution images of the digestive tract of free DiR and DiR-TH@PVP-gel at various time points after oral administration. (C) Representative *in vivo* fluorescence images of free DiR and DiR-TH@PVP-gel at various time points after oral administration. (D) Confocal images of DiI in the colon tissues of mice after treatment with free DiI or the DiI-TH@PVP-gel ($n = 3$ independent samples). Scale bar: 100 μm. (E) Fluorescence quantification of *ex vivo* biodistributed colon (left) and stomach (right) samples. (F) Fluorescence quantification of *in vivo* biodistribution. (G) Quantification of the fluorescence intensity of DiI. Data are shown as the mean ± SD.

colonic site was significantly enhanced by constructing the hydrogel delivery system, which was beneficial for further drug treatment. Similar conclusions could be drawn from *in vivo* imaging of the mice, in which free DiR gradually reached the colon in the first 10 h, and the total fluorescence intensity *in vivo* was significantly reduced at the 24th h. In contrast, DiR-loaded TH@PVP-gel still resulted in DiR accumulation in the colon at the 24th h (Figs. 6C and F). In addition, fluorescence quantification was also performed for other organs *ex vivo* during this time period, and the results, as shown in Fig. S11 (Supporting information), revealed that free DiR passed through the hepatic-intestinal circulation after oral administration, which caused a portion of the drug to accumulate in the liver, and finally some would reach the kidney; whereas the TH@PVP-gel released less free drug before it reached the colon site, and thus the accumulation in other organs was lower than that of free DiR. Next, to further examine the drug uptake by the cells at the colonic site, the colonic tissues were sectioned at 24 h after the oral administration of free DiI or the DiI-loaded TH@PVP-gel, and the fluorescence of the colonic tissues was photographed and quantified *via* confocal microscopy. The results, as shown in Figs. 6D and G, revealed that the accumulation of the DiI-loaded TH@PVP-gel in the colon was significantly greater than that of free DiI, which further demonstrated that the construction of the TH@PVP-gel could effectively enhance the ability of the drug to target the colonic tissues, thus achieving effective treatment of IBD.

On the basis of the increased colonic accumulation of the TH@PVP-gel in oral delivery applications and its excellent anti-inflammatory activity, and the multi-targeted anti-inflammatory mechanism was determined *via in vitro* experiments. Next, acute and chronic mouse models of colitis were constructed to assess whether the TH@PVP-gel could achieve a therapeutic effect in the complex inflammatory environment *in vivo*.

First, a model of acute colitis was constructed *via* the same method as that used for the biological distribution analysis, and oral administration of phosphate buffer saline (PBS), 5-ASA, Hem, Tan, a physical mixture of Hen and Tan, TH@PVP NPs, and TH@PVP-gel was given to each group simultaneously on days 1, 3, 5, and 7 during the modeling period. After the modeling and treatment were completed, on day 8, the colon and other relevant tissues were extracted out for further analysis (Fig. 7A). The distinguishing features of colitis include weight loss and shortened colon length. The changes in the body weight of the mice during treatment are shown in Fig. 7B, where a significant reduction in the body weight of the mice after DSS modeling was demonstrated, and both TH@PVP NPs and TH@PVP-gel presented excellent therapeutic effects compared with 5-ASA, which is currently a commonly used drug in the treatment of colitis. In addition, examination of the colon length led to the same conclusion, with the TH@PVP-gel having the strongest therapeutic effect relative to the other treatment groups (Figs. 7C and F). Furthermore, the pathological histology of the colon site was examined after treatment, and the TH@PVP-gel maximally ameliorated the pathological damage to the colon tissue. Specifically, after TH@PVP-gel treatment, the colonic crypt arrangement became ordered, the structure became more intact, and the degree of ulceration was significantly reduced (Fig. 7D). In addition, fibrosis and apoptosis of epithelial cells in colonic tissues were also examined *via* Masson and TUNEL staining (Fig. S12 in Supporting information), and the TH@PVP-gel effectively alleviated fibrosis as well as the degree of epithelial cell apoptosis.

Next, to further investigate how the TH@PVP-gel modulates the complex pathological environment of colitis *in vivo*, the anti-inflammatory mechanism of TH@PVP-gel was examined in a model of acute colitis. First, the modulation of neutrophils and macrophages by the TH@PVP-gel was examined, as shown in Fig. 7D and Fig. S13 (Supporting information). The IF results revealed that Tan could specifically induce neutrophil apoptosis, thus recruiting macrophages through cytosolic burial, whereas the TH@PVP-gel had a stronger effect than Tan on the basis of its ability to target drug release in the colon. Neutrophils, macrophages, and M2 macrophages were quantified *via* FACS, and as shown in Fig. 7E and Fig. S14 (Supporting information), the TH@PVP-gel maximally promoted cytosolic burial and further promoted macrophage M2 polarization on the basis of cytosolic burial and the anti-inflammatory mechanism of Hem and Tan. Moreover, the reduction of neutrophils was partly due to the apoptosis of neutrophils and efferocytosis of macrophages. TH@PVP-gel treatment also significantly restored colonic tight junctions and restored intestinal barrier damage caused by inflammation. Next, the level of oxidative stress in colonic tissues was examined after TH@PVP-gel treatment. ROS levels in the colon were first examined, and the TH@PVP-gel most effectively decreased ROS levels in the inflammatory environment (Fig. 7D and Fig. S13). Malondialdehyde (MDA) is a lipid peroxidation product, and as shown in Figs. 7G and H, the TH@PVP-gel most significantly decreased the level of oxidative stress due to intestinal inflammation. In addition, the total antioxidant capacity (T-AOC), catalase (CAT), glutathione peroxidase (GPx and SOD activities were also examined, and the results, as shown in Fig. 7I, revealed that TH@PVP-gel treatment most significantly enhanced the activity of the antioxidant system, which converts ROS into harmless substances, thus protecting cells from oxidative damage. We then analyzed the morphological changes of the intestinal tract to assess the mucosal recovery degree. As shown in Fig. S15 and Table S1 (Supporting information), control colon exhibited intact mucosal architecture with straight, well-organized crypts and abundant mucin-rich goblet cells. DSS treatment induced severe acute damage: crypts became fragmented and shortened with significant neutrophil infiltration, epithelial erosion, and goblet cell depletion, compromising mucosal barrier function. TH@PVP-gel intervention demonstrated

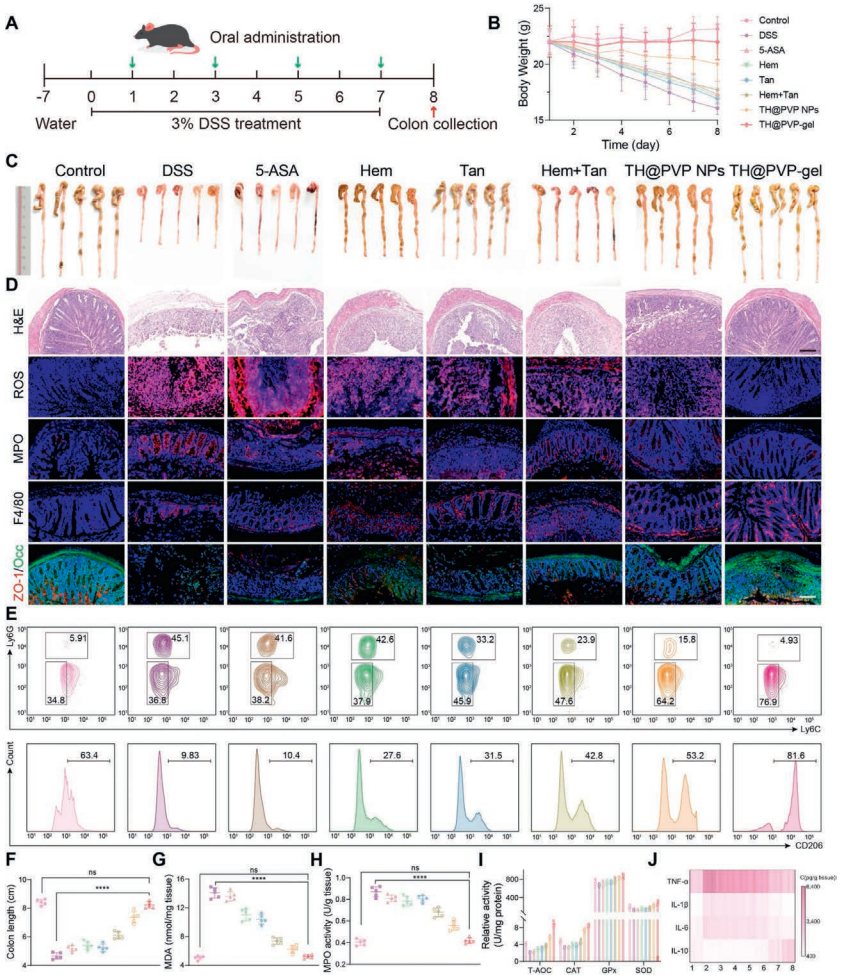


Fig. 7. Therapeutic efficacy of the TH@PVP-gel in the mice with DSS-induced acute colitis. (A) Schematic diagram of the experimental design. (B) Daily changes in body weight were recorded every day. (C) Images of the colon on day 8 in each group ($n = 5$ mice per group). (D) H&E and Masson staining, confocal images of ROS, MPO, F4/80, and ZO-1, and occludin in the colon tissues of each group ($n = 3$ independent samples). Scale bar: 100 μm. (E) The number of neutrophils/macrophages in the colon and the proportion of M2 macrophages in the colon were analyzed *via* FACS ($n = 3$ independent samples). (F) Colon lengths on day 8 after drug treatment, and MDA levels (G) and (H) MPO activity in each group after drug treatment ($n = 5$ independent samples). (I) Relative activity of T-AOC, CAT, GPx, and SOD in each group after drug treatment ($n = 5$ independent samples). (J) Heatmap of TNF-α, IL-1β, IL-6, and IL-10 expression profiles in serum ($n = 3$ independent samples). Data are shown as the mean ± SD (two-way ANOVA followed by Tukey's multiple comparisons *post hoc* test).

superior reparative effects, restoring near-normal crypt morphology and mucosal thickness while dramatically increasing goblet cell repopulation. Moreover, the serum levels of inflammatory factors were examined after treatment in each group, and the levels of tumor necrosis factor-alpha (TNF-α), interleukin 1β (IL-1β), and IL-6 were decreased and the level of IL-10 was increased after TH@PVP-gel treatment (Fig. 7J). Finally, the biosafety of the oral TH@PVP-gel was also examined; no significant histological damage to the organs was detected, and the serum biochemical parameters were within the normal range (Figs. S16 and S17 in Supporting information).

After acute colitis treatment, a model of DSS-induced chronic colitis was further constructed, and a treatment protocol was set up (Fig. 8A), with oral administration on days 1, 3, and 5 of every 6 days of DSS modeling, and the whole process was repeated in three rounds. Finally, the same test indices were used as those used for acute colitis. After treatment in each group, changes in body weight, pathological damage to colonic tissues, colonic length, tight junctions, neutrophils and macrophages, and oxidative stress levels were examined (Figs. 8B–J and Figs. S18–S23 in Supporting information). Chronic DSS exposure caused transmural pathology: Crypt atrophy with loss of glandular architecture, dense lymphoplasmacytic infiltration, submucosal fibrosis, and muscularis propria hyperplasia leading to marked wall thickening (Table S2 in Supporting information). While TH@PVP nanoparticles effectively targeted crypt regeneration and reduced collagen deposition, TH@PVP-gel achieved near-complete normalization of intestinal histology. It sustained crypt regeneration, suppressed fibroproliferation across mucosal and muscular layers, and reversed pathological wall thickening. As could be seen from the results, the systemic toxicity data of TH@PVP-gel was almost negligible and no obvious difference could be detected among different groups. Owing to the heterogeneity between chronic and acute colitis, the effects of 5-ASA, which is widely used in clinical practice, are different, with poorer therapeutic efficacy in chronic inflammation than in acute inflammation. In addition, the effects of Hem and Tan monotherapy also differ from those in acute inflammation. In contrast, the multi-target effects of the TH@PVP-gel in the treatment of chronic inflammation in different inflammatory environments compared with in acute inflammation simultaneously address both the heterogeneity and commonality of different inflammatory environments. TH@PVP-gel efficiently scavenges ROS, attenuates the extent of colonic apoptosis, and downregulates the level of chronic inflammatory fibrosis while modulating neutrophils and macrophages. Compared with single-agent therapy, the TH@PVP-gel has superior therapeutic efficacy in both acute

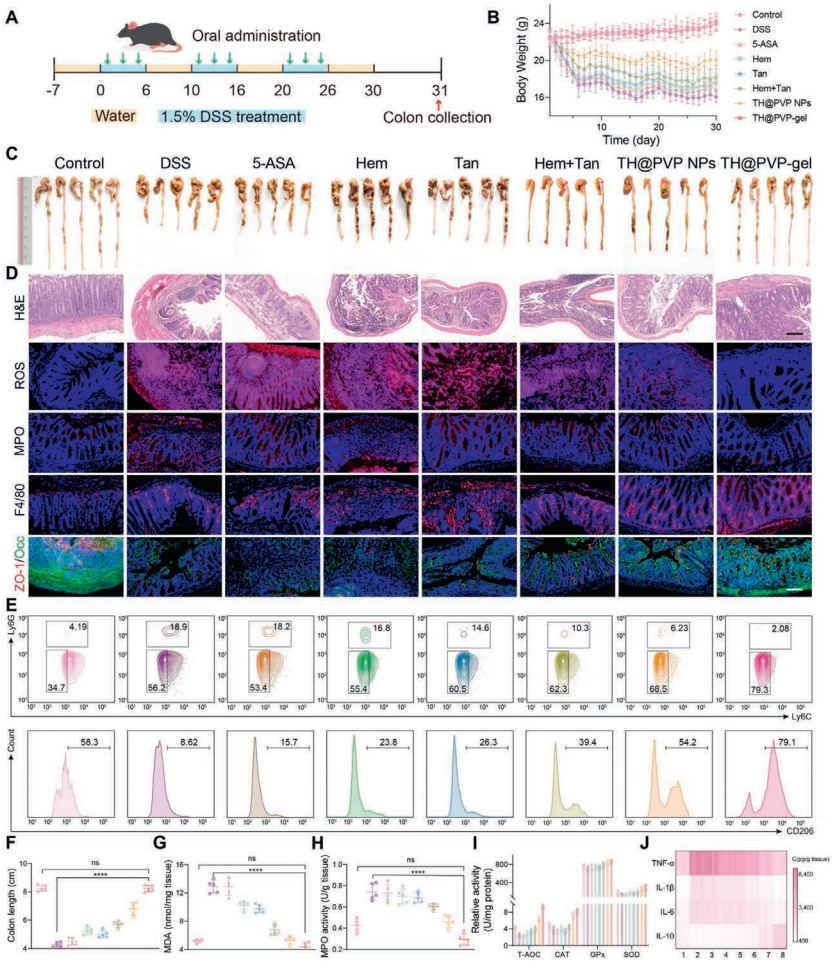


Fig. 8. Therapeutic efficacy of the TH@PVP-gel in the mice with DSS-induced chronic colitis. (A) Schematic diagram of the experimental design. (B) Daily changes in body weight were recorded every day. (C) Images of the colon on day 8 in each group ($n = 5$ mice per group). (D) H&E and Masson staining, confocal images of ROS, MPO, F4/80, ZO-1, and occludin in the colon tissues of each group ($n = 3$ independent samples). Scale bar: 100 μm. (E) The number of neutrophils/macrophages in the colon and the proportion of M2 macrophages in the colon were analyzed *via* FACS ($n = 3$ independent samples). (F) Colon lengths on day 8 after drug treatment ($n = 5$ independent samples). MDA levels (G) and (H) MPO activity in each group after drug treatment ($n = 5$ independent samples). (I) Relative activity of T-AOC, CAT, GPx, and SOD in each group after drug treatment ($n = 5$ independent samples). (J) Heatmap of TNF-α, IL-1β, IL-6, and IL-10 expression profiles in serum ($n = 3$ independent samples). Data are shown as the mean ± SD (two-way ANOVA followed by Tukey's multiple comparisons *post hoc* test).

and chronic colitis because of its multi-target effects on the inflammatory milieu and its ability to release drugs in a colon-targeted manner.

With the great advancement of combing machine learning, high-throughput screening and anti-oxidative therapy, the therapeutical effect on IBD is largely increased [49,50]. However, current therapeutic strategies for IBD, including corticosteroids, immunomodulators, and biologics, remain constrained by suboptimal efficacy in both induction and maintenance phases, coupled with risks of treatment resistance, dependency, and adverse effects. A significant subset of patients fails to achieve durable mucosal healing despite aggressive therapies, perpetuating cycles of relapse and elevating susceptibility to long-term complications. These limitations underscore the urgent need for novel approaches addressing the pathophysiological heterogeneity of IBD, particularly the dynamic interplay between innate immune dysregulation and epithelial barrier dysfunction. Emerging evidence highlights distinct immune microenvironmental signatures in acute *versus* chronic inflammation, characterized by divergent neutrophil infiltration levels and macrophage polarization states. This biological heterogeneity necessitates therapeutic strategies capable of adaptively modulating immune responses across disease stages.

We developed TH@PVP-gel, an orally administered hydrogel platform engineered to target multiple pathological axes of IBD. TH@PVP-gel exhibits potent ROS scavenging capacity *in vitro* and *in vivo*, thereby mitigating oxidative stress-induced epithelial apoptosis and restoring intestinal barrier integrity. Notably, the hydrogel displays microenvironment-responsive immunomodulatory properties: under inflammatory conditions, it selectively induces neutrophil apoptosis, a critical mechanism for resolving acute inflammation, while concurrently promoting macrophage repolarization toward the M2 phenotype. This dual action facilitates transition from a pro-inflammatory to a pro-reparative milieu, addressing both acute exacerbations and chronic inflammatory remodeling.

The therapeutic superiority of TH@PVP-gel was evident in experimental models of acute and chronic colitis, where it achieved comprehensive mucosal remission-a clinical endpoint rarely attained with conventional monotherapies. By synchronously targeting epithelial survival, oxidative stress, and innate immune cell dynamics, this approach circumvents the mechanistic limitations of current treatments that often focus on single inflammatory pathways. Importantly, the oral route of administration and localized action of TH@PVP-gel may reduce systemic immunosuppressive risks associated with biologics or small-molecule inhibitors.

Declaration of competing interest

The authors declare that they have no known competing financial interests or personal relationships that could have appeared to influence the work reported in this paper.

CRediT authorship contribution statement

Yu-Yang Bi: Writing – review & editing, Writing – original draft, Visualization, Validation, Software, Resources, Project administration, Methodology, Investigation, Formal analysis, Data curation, Conceptualization. **Ling-Feng Zhang:** Writing – review & editing, Visualization, Validation. **Qiu Chen:** Project administration, Methodology, Investigation. **Ming-Yuan Yang:** Writing – review & editing, Project administration. **Lei Xing:** Supervision, Funding acquisition, Conceptualization. **Hu-Lin Jiang:** Writing – review & editing, Writing – original draft, Supervision, Resources, Funding acquisition. **Xian-Wu Cheng:** Supervision, Resources, Funding acquisition.

Acknowledgments

This work was financially supported by the National Natural Science Foundation of China (Nos. 82020108029, 82073398, 823023677, 82473867, 82370424), the National Key R&D Program of China (No. 2022YFE0198400), the Leading Technology Foundation Research Project of Jiangsu Province (No. BK20192005), Natural Science Foundation of Basic Research Program - Project Jointly Funded by Province and City (No. BK20232035), Haihe Laboratory of Cell Ecosystem Innovation Fund (No. 22HHXBSS00005), Nanjing Scientific and Technological Special Project for Life and Health (No. 202110006), and the Jilin Provincial Foundation of Changbai Talent Outstanding Team (No. 202410006). The authors thank Xiao-Nan Ma for providing technical assistance of confocal microscopy work on the Public Laboratory Platform of China Pharmaceutical University.

Supplementary materials

Supplementary material associated with this article can be found, in the online version, at doi:10.1016/j.cclet.2025.111836.

References

[1] B. Gros, G.G. Kaplan, JAMA 330 (2023) 951–965.
[2] G.G. Kaplan, Nat. Rev. Gastro. Hepat. 12 (2015) 720–727.
[3] H. Everhov Å, J. Halfvarson, P. Myrelid, et al., Gastroenterology 154 (2018) 518–528.
[4] E. Louis, J.Y. Mary, G. Vernier-Massouille, et al., Gastroenterology 142 (2012) 63–70.
[5] S. Honap, V. Jairath, S. Danese, L. Peyrin-Biroulet, Nat. Rev. Drug Discov. 23 (2024) 546–562.
[6] P.S. Dulai, S. Singh, V. Jairath, E. Wong, N. Narula, Gastroenterology 166 (2024) 396–408.
[7] B. Verstockt, M. Parkes, J.C. Lee, Gastroenterology 162 (2022) 1383–1395.
[8] J.T. Chang, NEJM 383 (2020) 2652–2664.
[9] C. Danne, J. Skerniskyte, B. Marteyn, H. Sokol, Nat. Rev. Gastro. Hepat. 21 (2024) 184–197.
[10] S. Wang, Y. Song, Z. Wang, et al., Cell. Mol. Immunol. 21 (2024) 620–633.
[11] L.M. Hegarty, G.R. Jones, C.C. Bain, Nat. Rev. Gastro. Hepat. 20 (2023) 538–553.
[12] Y.R. Na, M. Stakenborg, S.H. Seok, G. Matteoli, Nat. Rev. Gastro. Hepat. 16 (2019) 531–543.
[13] C. Glorieux, S. Liu, D. Trachootham, P. Huang, Nat. Rev. Drug Discov. 23 (2024) 583–606.
[14] L.A. O'Neill, R.J. Kishton, J. Rathmell, Nat. Rev. Immunol. 16 (2016) 553–565.
[15] J. Zhou, C. Fang, C. Rong, et al., Smart Mater. Med. 4 (2023) 427–446.
[16] A. Garrido-Trigo, A.M. Corraliza, M. Veny, et al., Nat. Commun. 14 (2023) 4506.
[17] J. Lu, X. Shen, H. Li, J. Du, Exploration 4 (2024) 20230142.
[18] R. Han, Z. Ren, Q. Wang, et al., Adv. Sci. 11 (2024) e2308325.
[19] B. Park, G. Han, D.Y. Jin, et al., ACS Nano 18 (2024) 16297–16311.
[20] X. Yan, J. Song, Y. Zhang, et al., Nano Today 54 (2024) 102139.
[21] Z. Li, H. Shen, W. Cai, et al., Chin. Chem. Lett. 37 (2026) 111292.
[22] C. Zhang, J. Li, M. Xiao, et al., Chin. Chem. Lett. 33 (2022) 4924–4929.
[23] Y. Yan, J. Song, D. Liu, et al., Chin. Chem. Lett. 35 (2024) 109736.
[24] J. Ge, B. Jia, Y. Wang, et al., Adv. Funct. Mater. 34 (2024) 2402781.
[25] D.K. Min, Y.E. Kim, M.K. Kim, et al., ACS Nano 17 (2023) 24404–24416.
[26] J. Yu, S. Li, B. Xiong, et al., Adv. Mater. 37 (2025) e2412429.
[27] G. Zhang, D. Song, R. Ma, et al., Sci. Adv. 10 (2024) eado8222.
[28] S. Gao, H. Zheng, S. Xu, et al., Adv. Healthc. Mater. 12 (2023) e2301826.
[29] L. Quan, Y. Ouyang, W. Liang, et al., Adv. Sci. 27 (2025) e04802.
[30] Y. Chen, M. Shui, H. Li, et al., Biomaterials 318 (2025) 123163.
[31] W. Chen, Y. Xu, H. Li, et al., ACS Appl. Mater. Interfaces 12 (2020) 21470–21480.
[32] A.L. Robertson, G.R. Holmes, A.N. Bojarczuk, et al., Sci. Transl. Med. 6 (2014) 225ra229.
[33] Y. Gong, Y.L. Zhang, Z. Wang, et al., J. Neuroinflamm. 17 (2020) 198.
[34] M. Lian, Z. Xue, X. Qiao, et al., Chem 5 (2019) 2378–2387.
[35] Z. Wei, Y. Zhang, L. Wang, et al., ACS Appl. Mater. Interfaces 13 (2021) 32316–32331.
[36] Z. Wu, L. Chen, W. Guo, et al., Nat. Nanotechnol. 19 (2024) 1375–1385.
[37] N.J. Hunt, G.P. Lockwood, S.J. Heffernan, et al., Nat. Nanotechnol. 19 (2024) 534–544.
[38] X. Zhang, G. Chen, H. Zhang, L. Shang, Y. Zhao, Nat. Rev. Bioeng. 1 (2023) 208–225.
[39] Z. Wang, Z.X. Wang, K.F. Xu, et al., Adv. Mater. 37 (2024) e2410993.
[40] B. Deng, S. Liu, Y. Wang, et al., Adv. Mater. 36 (2024) 2306081.
[41] Y. Hu, S.Y. Tzeng, L. Cheng, et al., Proc. Natl. Acad. Sci. U. S. A. 121 (2024) e2400194121.
[42] H. Li, X. Qian, H. Mohanram, et al., Nat. Nanotechnol. 19 (2024) 1141–1149.
[43] X. Guo, W. Luo, L. Wu, et al., Adv. Sci. 11 (2024) e2403388.
[44] X. Zheng, Q. Tong, L. Ma, et al., Chem. Eng. J. 500 (2024) 157090.
[45] R. Luo, J. Liu, Q. Cheng, et al., Sci. Adv. 10 (2024) eado6798.
[46] X. Zhang, Z. Yuan, J. Wu, et al., ACS Nano 17 (2023) 21116–21133.
[47] Y. Ma, S. Gou, Z. Zhu, et al., Adv. Mater. 36 (2024) e2309516.
[48] L. Lei, Q. Tu, L. Jiao, et al., Chem. Eng. J. 432 (2022) 134356.
[49] Y. Yu, X. Zhao, X. Xu, et al., Adv. Mater. 35 (2023) e2304967.
[50] X. Zhao, Y. Yu, X. Xu, et al., Adv. Mater. 37 (2025) e2417536.